JSES International 8 (2024) 851–858

Contents lists available at ScienceDirect

JSES International

journal homepage: www.jsesinternational.org

A stemless anatomic shoulder arthroplasty design provides increased cortical medial calcar bone loading in variable bone densities compared to a short stem implant

Daniel Ritter, MSc[a,b,*], Patrick J. Denard, MD[c], Patric Raiss, MD[d], Coen A. Wijdicks, PhD, MBA[a], Samuel Bachmaier, MSc[a]

[a]Arthrex Department of Orthopedic Research, Munich, Germany
[b]Department of Orthopaedics and Trauma Surgery, Musculoskeletal University Center Munich (MUM), University Hospital, LMU Munich, Munich, Germany
[c]Southern Oregon Orthopedics, Medford, OR, USA
[d]OCM Clinic, Munich, Germany

ARTICLE INFO

Keywords:
Stemless TSA
Humeral implant micromotion
Medial calcar bone loading
Cortical rim support
Bone density
Biomechanics

Level of evidence: Basic Science Study; Biomechanics

Background: Several studies have reported proximal bone resorption in stemless and press-fit short-stem humeral implants for anatomic total shoulder arthroplasty. The purpose of this biomechanical study was to evaluate implant and cortical bone micromotion of a cortical rim-supported stemless implant compared to a press-fit short stem implant during cyclic loading and static compression testing.
Methods: Thirty cadaveric humeri were assigned to 3 groups based on a previously performed density analysis, adopting the metaphyseal and epiphyseal and inferior supporting bone densities for multivariate analyses. Implant fixation was performed in stemless implant in low bone density (SL-L, n = 10) or short stem implant in low bone density (Stem-L, n = 10) and in stemless implant in high bone density (SL-H, n = 10). Cyclic loading with 220 N, 520 N, and 820 N over 1000 cycles at 1.5 Hz was performed with a constant valley load of 25 N. Optical recording allowed for spatial implant tracking and quantification of cortical bone deformations in the medial calcar bone region. Implant micromotion was measured as rotational and translational displacement. Load-to-failure testing was performed at a rate of 1.5 mm/s with ultimate load and stiffness measured.
Results: The SL-H group demonstrated significantly reduced implant micromotion compared to both low-density groups (SL-L: $P = .014$; Stem-L: $P = .031$). The Stem-L group showed significantly reduced rotational motion and variance in the test results at the 820-N load level compared to the SL-L group (equal variance: $P = .012$). Implant micromotion and reversible bone deformation were significantly affected by increasing load ($P < .001$), metaphyseal cancellous ($P = .023$, $P = .013$), and inferior supporting bone density ($P = .016$, $P = .023$). Absolute cortical bone deformation was significantly increased with stemless implants in lower densities and percentage reversible bone deformation was significantly higher for the SL-H group (21 ± 7%) compared to the Stem-L group (12 ± 6%, $P = .017$).
Conclusion: A cortical rim-supported stemless implant maintained proximally improved dynamic bone loading in variable bone densities compared to a press-fit short stem implant. Biomechanical time-zero implant micromotion in lower bone densities was comparable between short stem and stemless implants at rehabilitation load levels (220 N, 520 N), but with higher cyclic stability and reduced variability for stemmed implantation at daily peak loads (820 N).

Anatomic total shoulder arthroplasty (aTSA) has historically demonstrated acceptable results. In an effort to preserve bone and improve revisability, the humeral component has transitioned towards short-stem and stemless designs. However, bone resorption can occur from unphysiological proximal humeral bone loading. While particularly stemmed and short stem designs have shown

Institutional review board approval was not required for this study.
Investigation performed at the Arthrex Department of Orthopedic Research, Munich, Germany.

*Corresponding author: Daniel Ritter, MSc, Arthrex GmbH Department of Orthopedic Research, Erwin-Hielscher-Strasse 9, Munich 81249, Germany.
E-mail address: publications@arthrex.com (D. Ritter).

https://doi.org/10.1016/j.jseint.2024.02.008

resorptions in the medial calcar region,[14,32,37] similar bone resorptions were found for metaphyseal impacted fin designs ,[1-3,11,19] while a hollow screw design rather reduced the cancellous bone density in the greater tuberosity region.[20,21] While the short-term clinical impact of such stress shielding is minimal,[1,20,21,23,39] potential longer term drawbacks may include survival time, long-term outcomes, bone loss affecting revision, and periprosthetic fracture.[16] The additional influence of low bone mineral density (BMD) also remains unclear in these cases. As stemless implants are increasingly used in a wider range of bone quality, there is substantial interest in objective predictions of stemless implants in aTSA using bone density evaluations in the proximal humerus.[13,22,26]

Biomechanical studies in these settings have mainly focused on primary stability and micromotion measurements, without considering effects on humeral bone loading.[3,10,17] Physiological load transfer patterns in the healthy proximal humerus are complex with respect to specific arm movements and have been shown to vary between poor and normal bone quality, highlighting the importance of cortical load absorption.[18,28,33] Finite element analyses (FEA) of stemless implants have also confirmed the importance of cortical load transfer to increase stability and mimic native humeral loads.[33,34] Cortical loading varies by implant design. For instance, a reduction of medial calcar stress shielding has been reported using a central screw design with cortical rim support that maintains bone loading similar to physiological stresses.[1,2,27] Further experimental investigation of the implant-bone interface, including micromotion and bone deformation analyses, may thus help to better understand the differences in the implant-to-bone load transfer of different implant types.

The purpose of this biomechanical study was to evaluate implant and cortical bone micromotion during cyclic loading and static compression testing of a cortical rim-supported stemless implant compared to an press-fit short stem implant. We hypothesized that a cortical rim-supported stemless design would provide similar stability compared to an impacted short stem implant in variable bone densities but with optimized bone loading in the medial proximal humerus.

Materials and methods

A biomechanical investigation was performed on 30 fresh-frozen cadaveric proximal humeri specimens (68.3 ± 11.5 years; 13 females 17 males) (Science Care Inc., Phoenix, AZ, USA). For all cadavers, there was no sign of degenerative joint disease. The specimens were assigned to low- and high-density groups based on computed tomography (CT) scans and a classification model using the thresholds trained in a previous work.[35] Ten specimens were classified as high bone density and 20 were classified as low bone density. A stemless humeral implant (Eclipse; Arthrex Inc., Naples, FL, USA) was implanted in the stemless implant in high bone density (SL-H, n = 10). The 20 low-density cadavers were randomly assigned to either receive the same stemless implant in low bone density (SL-L, n = 10), or a short stem porous coated press-fit implant (Apex OptiFit Humeral Stem; Arthrex Inc., Naples, FL, USA) (Stem-L, n = 10).

Surgical technique

Specimens were stored at −20° C and thawed overnight at room temperature before tissue preparation and testing. After identifying the humeral neck based on anatomic landmarks the humeral head was resected along the anatomic neck perpendicular to the metaphyseal axis using an oscillating saw and a cutting guide. For stemless implantation the proximal humerus was measured, and a cortical rim-supported trunnion was placed followed by compression with a hollow cage screw along the metaphyseal axis according to the manufacturer's recommendations. Cortical rim support at the medial calcar was ensured by sizing the trunnion to the outer rim of the humeral head cut. Short stem cementless press-fit implantation was performed by broaching the humeral canal according to the manufacturer's recommendations.

Bone density

Bone density parameters were adopted from a previous study, with humeral bones scanned by a standard clinical CT (Siemens SOMATOM Definition AS+; Siemens Healthcare GmbH, Erlangen, Germany) with a voxel resolution of 0.6 × 0.6 × 0.6 mm. Standard calibration according to the manufacturer's protocol using density phantoms [0; 200 mgHA/cm^3] was performed to allow conversion of gray scale values to BMD (mgHA/cm^3) as well as to ensure consistency between CT scans. All CT voxel data were imported as a 4-dimensional point cloud (ie [x, y, z, mgHA/cm^3]) and the slices were initially oriented parallel to the anatomical neck for region of interest analysis. Evaluation using a custom image processing script (MathWorks, Natick, MA, USA) allowed for the adoption of the following parameters for previously described stemless aTSA classification (Fig. 1).[35]

Biomechanical testing

Based on prior biomechanical studies, 3 load steps were applied, loading to 220 N, 520 N, and 820 N.[6,7,10,17,41] The lower load level (220 N) was applied to simulate 20% body weight (196 N) for rehabilitation arm movements measured by a telemetric shoulder implant.[6] The middle load step (520 N) simulated loads during the first 2 months of physiotherapy after shoulder arthroplasty, representing 40% body weight (392 N) during training against resistance.[6] Peak loads during "normal" use with no weight in the hand were simulated by the upper load block (820 N) as the worst case scenario during rehabilitation. Loads were applied in the coronal plane at an angle of 30° from the central axis of the implant, as demonstrated by in vivo measurements.[7,41] Loads were applied cyclically to the humeral head using a custom-made polyethylene (PE) stamp with the respectively sized PE glenoid curvature to simulate contact pressure for 1000 cycles per load block in force control mode at 1.5 Hz (Fig. 2, *A*). Loads were applied using a single axis material testing machine (ElectroPuls E3000; Instron, Norwood, MA, USA) to investigate micromotion and bone deformation at the steady states within the last cycle of each load block using an optical tracking system (Fig. 2, *B*). Additional static loading was performed at a rate of 1.5 mm/s after cyclic loading. Mechanical data were recorded continuously with a sampling rate of 500 Hz. All tests were performed at room temperature and the tissue was kept moist with physiological saline solution throughout preparation and testing.

Implant–bone interface analysis

Micromotion of the implant in reference to the bone and bone deformation was recorded using an optical tracking system (Carl Zeiss GOM Metrology GmbH, Braunschweig, Germany). Tracking points (diameter 0.8 mm) were fixed on the embedding, bone, implant, and actuator, respectively allowing for rigid body motion correction in reference to the fixed embedding. The systems' use of 2 cameras allowed for spatial point cloud tracking with a mean deviation of 5.4 ± 2.8 μm. Tracking of the point clouds attached along the cortical margin 2 mms below the resection plane allowed for measurement of the cortical superficial bone deformation. The separation in relative implant and bone motion was achieved by the application of different coordinate systems for each component applied in the optical tracking system. Images were either

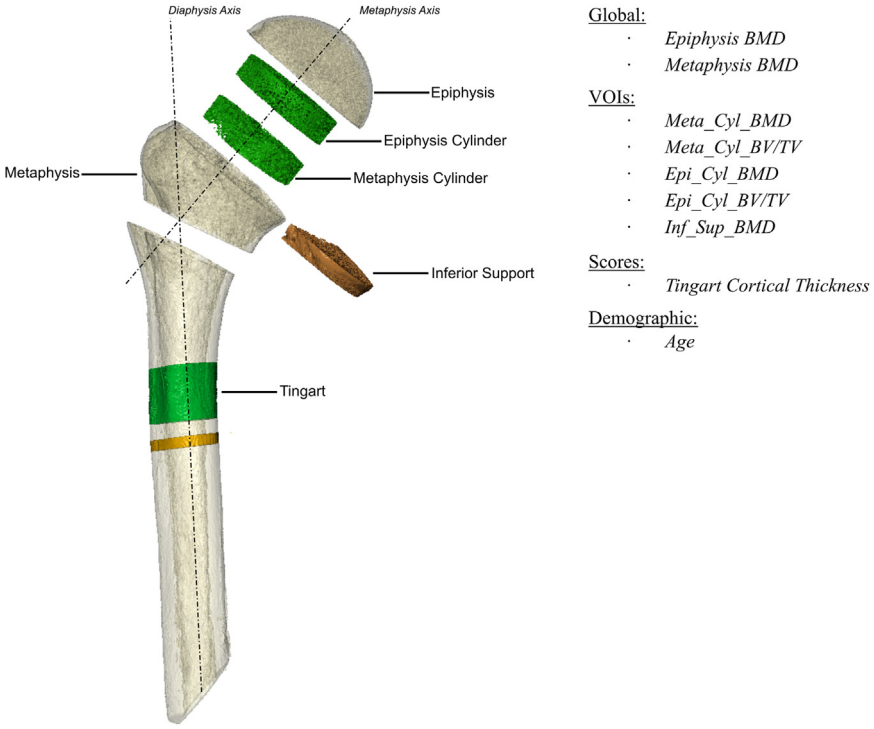

Figure 1 Adopted bone density variables from a previous work.
(Reprinted from Ritter et al[35]) © 2024 Journal of Shoulder and Elbow Surgery Board of Trustees. *BMD*, bone mineral density; *BV/TV*, bone volume/total volume.

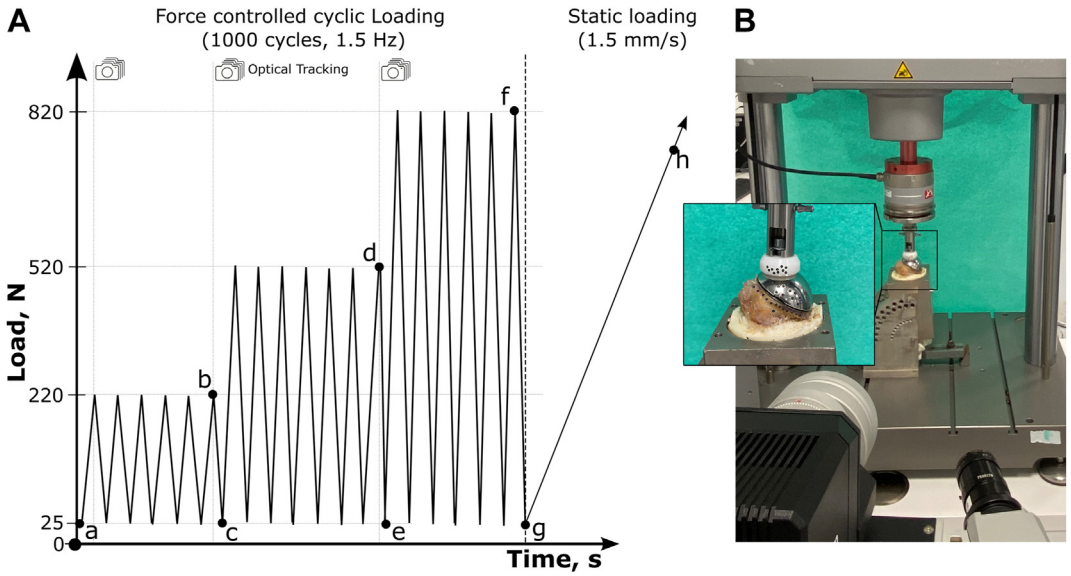

Figure 2 (**A**) Testing protocol and (**B**) experimental cyclic loading and static loading setup including the camera setup and tracking points. Points of data analysis included total cyclic deformation measurements (s_{tot}, Δab, Δad, and Δaf) at the end of each load block. During the final hysteresis in each loading block using the tracking points, micromotion (Δbs, Δde, and Δfg) was evaluated and further divided into the motion of the implant ($s_{Implant}$, $\alpha_{Implant}$) and compressive transmission caused deformation of the bone (s_{Bone}). Ultimate load and stiffness were analyzed during final static compression testing (F_{max}, D_{UF}; Δgh).

compared to the time-zero reference state or evaluated during applied load hystereses (Fig. 3). Optical measurements were taken at a sampling rate of 30 Hz.

Outcome data

Metrics for comparison included data from cyclic loading and static compression testing. Cyclic outcome variables included the total construct displacement (s_{tot}) at the end of each loading block (220 N, 520 N, and 820 N). At the same time, micromotion during one loading hysteresis (Fig. 3) additionally provided relative information about implant micromotion ($s_{Implant}$, $\alpha_{Implant}$) and compression-induced superficial deformation of the medial calcar cortical bone (s_{Bone}). To further investigate the load absorption capability of the bone, the measured superficial cortical deformation was related to the total displacement as a percentage. The

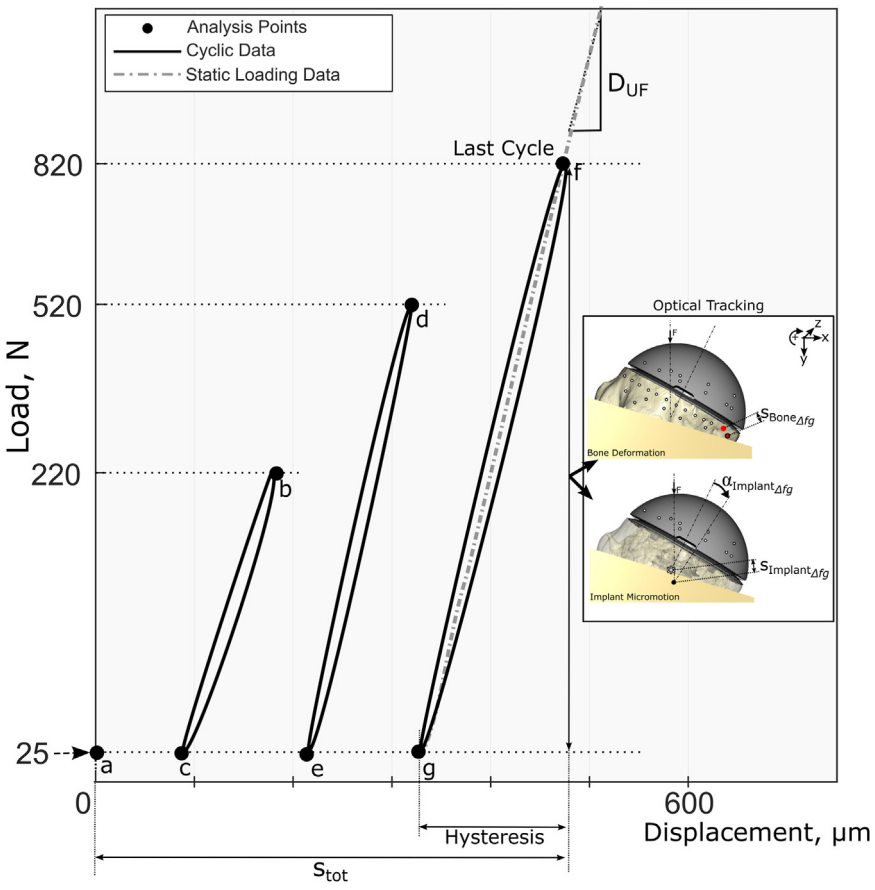

Figure 3 Schematic illustration of representative load-displacement curves at the end of each load block for total deformation measurement (s_{tot}) including optical tracking for micromotion analysis during reversible hysteresis loading dividing up in implant motion ($s_{Implant}$, $\alpha_{Implant}$) and bone deformation (s_{Bone}). Ultimate load and stiffness (D_{UF}) were analyzed during static compression testing.

ultimate load (F_{max}) was defined directly after the elastic progression where the linear stiffness (D_{UF}) was determined during the static compression test. Data analysis was performed with commercial software (Matlab version R2019a; MathWorks, Natick, MA, USA).

Statistical analysis

Biomechanical testing outcome metrics were the dependent primary outcome variables. Bone density variables were defined as secondary outcome variables and were used as covariates in multivariable regression analyses. Statistical analysis was performed using commercial software (Sigma Plot Statistics for Windows, version 13.0; Systat Software, San Jose, CA, USA).

The statistical analysis included a 1-way analysis of variance with a Holm-Sidak post hoc test performed for a significant pairwise analysis of primary outcome variables. Significance was defined as $P \leq .05$ and the desired power level was set at 0.8. Post hoc power analysis was performed to confirm adequate sample size. The Shapiro–Wilk test and Brown–Forsythe test were used to confirm each data set followed a normal distribution and equal variance, respectively. A nonparametric test (Kruskal–Wallis) was used for data sets that failed these tests. For Kruskal–Wallis tests that found significance, a post hoc test acc. to Dunn's method was conducted to further analyze the differences. The observed post hoc average power values of all 1-way analysis of variance tests were higher than the desired power level of 0.8 leading us to conclude that our sample size was sufficient.

A 1-way analysis of covariance for multivariable regression analysis including the adopted density variables [35] was performed to quantify interactions and compare the groups with each other. For analysis of covariance tests that were considered significant in an equal slope model, a Holm Sidak post hoc test was performed for pairwise analysis. Significance was defined as $P \leq .05$ and the desired power level was set at 0.8. The Shapiro–Wilk and Levene tests were used to confirm each data set followed a normal distribution and homogeneity in variance, respectively.

Results

Bone density variables are summarized in Table I.

Cyclic testing

Cyclic displacement was lowest in the SL-H group (Fig. 4). At the highest load level, the SL-L group showed significantly increased total displacement (436 ± 172 µm) compared to the Stem-L (370 ± 90 µm, $P = .003$) and SL-H (226 ± 92 µm, $P = 02$) groups, which were also significantly different ($P = .044$).

Absolute bone deformation was significantly increased for the SL-L group (520 N: 39 ± 10 µm; 820 N: 64 ± 22 µm) compared to the stemmed implant (520 N: 22 ± 13 µm; 820 N: 38 ± 23 µm) in the 520 N and 820 N load blocks (Fig. 5). The percentage of reversible bone deformation for the SL-H group (21 ± 7%, $P = .017$) was significantly higher at all load levels compared to the Stem-L group (12 ± 6%). SL-L maintained a percentual bone deformation of

Table I
Mean values with standard deviations of the density variables (BMD: Bone Mineral Density; BV/TV: Bone Volume/Total Volume) for specimens assigned to the stemless or stemmed group including statistical analysis.

	SL-L	SL-H	Stem-L	SL-L vs. SL-H	Stem-L vs. SL-H	Stem-L vs. SL-L
				P value	*P* value	*P* value
Epiphysis BMD [mgHA/cm^3]	324 ± 43	412 ± 31	332 ± 31	***<.001***	***<.001***	*.831*
Metaphysis BMD [mgHA/cm^3]	343 ± 37	410 ± 35	354 ± 34	***.003***	***.002***	*.759*
Epiphysis Cylinder BMD [mgHA/cm^3]	282 ± 24	323 ± 17	280 ± 23	***<.001***	***<.001***	*.123*
Epiphysis Cylinder BV/TV	0.38 ± 0.21	0.44 ± 0.20	0.37 ± 0.19	***.007***	***.011***	*.970*
Metaphysis Cylinder BMD [mgHA/cm^3]	260 ± 9	297 ± 14	265 ± 12	***.003***	***.002***	*.662*
Metaphysis Cylinder BV/TV	0.20 ± 0.11	0.33 ± 0.11	0.19 ± 0.11	***.001***	***.004***	*.927*
Inferior Support BMD [mgHA/cm^3]	333 ± 38	412 ± 31	351 ± 35	***<.001***	***.001***	*.480*
Tingart Cortical Thickness [mm]	3.1 ± 0.4	3.6 ± 0.4	3.1 ± 0.4	***.005***	***.009***	*.939*
Age [y]	73.1 ± 9.4	60.7 ± 9.5	72.2 ± 11.6	***.021***	***.029***	*.977*

SL-L, stemless implant in low bone density; *SL-H*, stemless implant in high bone density; *Stem-L*, short stem implant in low bone density; *BMD*, bone mineral density; *BV/TV*, bone volume/total volume.
Italic bold = significant ($P < .05$) and italic = not significant ($P > .05$).

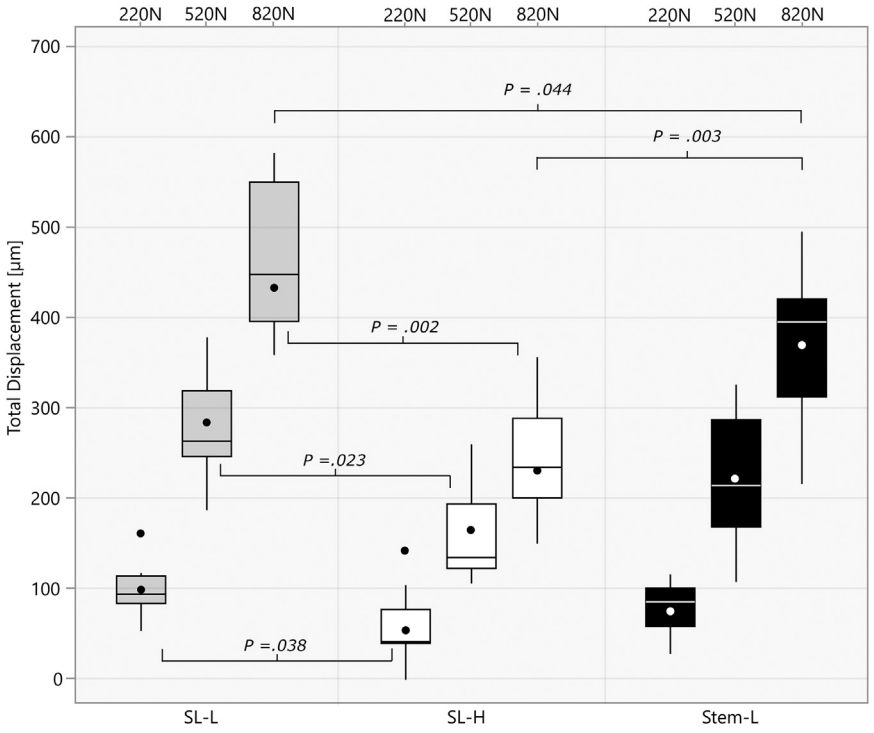

Figure 4 Boxplot with mean and median overall cyclic displacement at the end of the cyclic loading blocks (220 N, 520 N, and 820 N). *SL-L*, stemless implant in low bone density; *SL-H*, stemless implant in high bone density; *Stem-L*, short stem implant in low bone density.

19 ± 7% without significant differences to the SL-H ($P = .110$) and Stem-L group ($P = .669$).

Significantly increased implant micromotion (Fig. 6, *A*) occurred at the highest load level in the lower bone density groups (SL-L 232 µm (confidence interval [CI]95:98-341 µm), $P = .015$ and Stem-L 221 µm (CI95:118-244 µm), $P = .038$) compared to the SL-H group (122 µm (CI95:93-236 µm)). The SL-H and Stem-L groups showed significantly reduced rotational motion (Fig. 6, *B*) at the 820-N load level compared to the SL-L group (Equal variance: $P = .012$) with lower variance in the test results for the Stem-L group.

Covariance with bone densities

Implant micromotion interacted significantly with the increasing load ($P < .001$), metaphyseal cancellous bone density ($P = .023$), and inferior supporting bone density ($P = .016$). Implant micromotion was significantly reduced in the SL-H group compared to both low-density groups (SL-L: $P = .014$; Stem-L: $P = .031$), which were not significantly different ($P = .274$).

Bone deformation significantly interacted with increasing load ($P < .001$), cancellous epiphyseal ($P = .019$) and metaphyseal bone density ($P = .013$), and inferior supporting bone density ($P = .023$). The SL-L group showed significantly more bone deformation than the Stem-L group ($P = .021$).

Static loading

All constructs reached the regular test end and were statically loaded. The linear stiffness of the stem group (1328 ± 282 N/mm) was significantly decreased compared to stemless groups in high (1641 ± 285 N/mm, $P = .026$) and low bone densities (1623 ± 246 N/mm, $P = .046$), which did not differ significantly to each other ($P = .680$). The ultimate loads did not differ significantly between the groups ($P = .330$) with a mean load of 2506 ± 298 N.

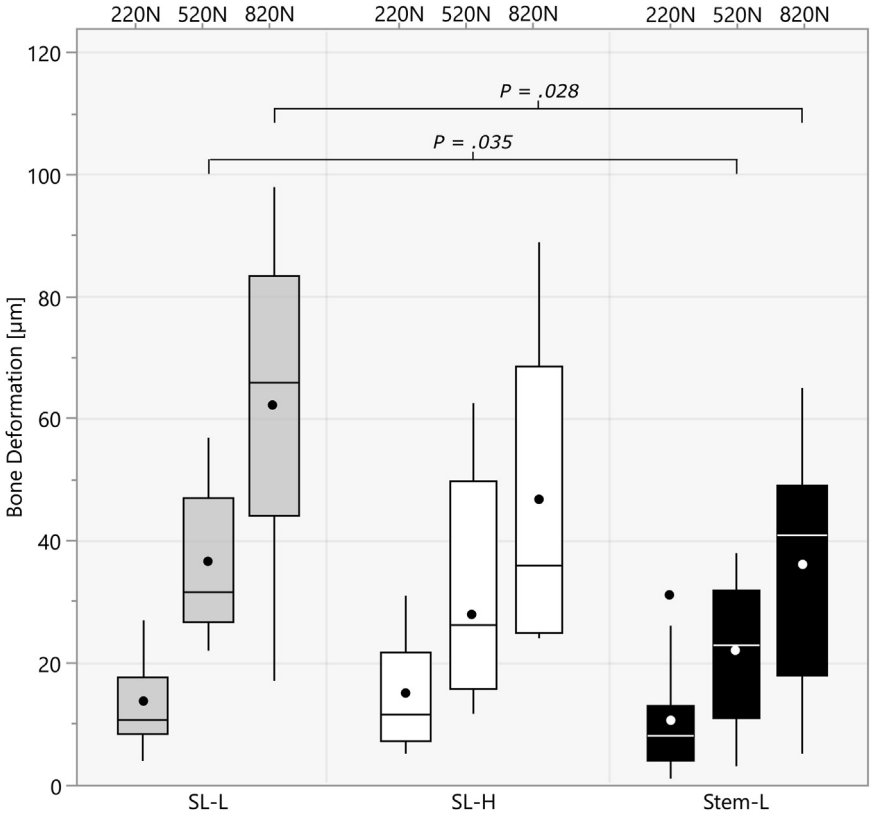

Figure 5 Boxplot with mean and median bone deformations during hysteresis loading at the end of each cyclic loading block (220 N, 520 N, and 820 N). *SL-L*, stemless implant in low bone density; *SL-H*, stemless implant in high bone density; *Stem-L*, short stem implant in low bone density.

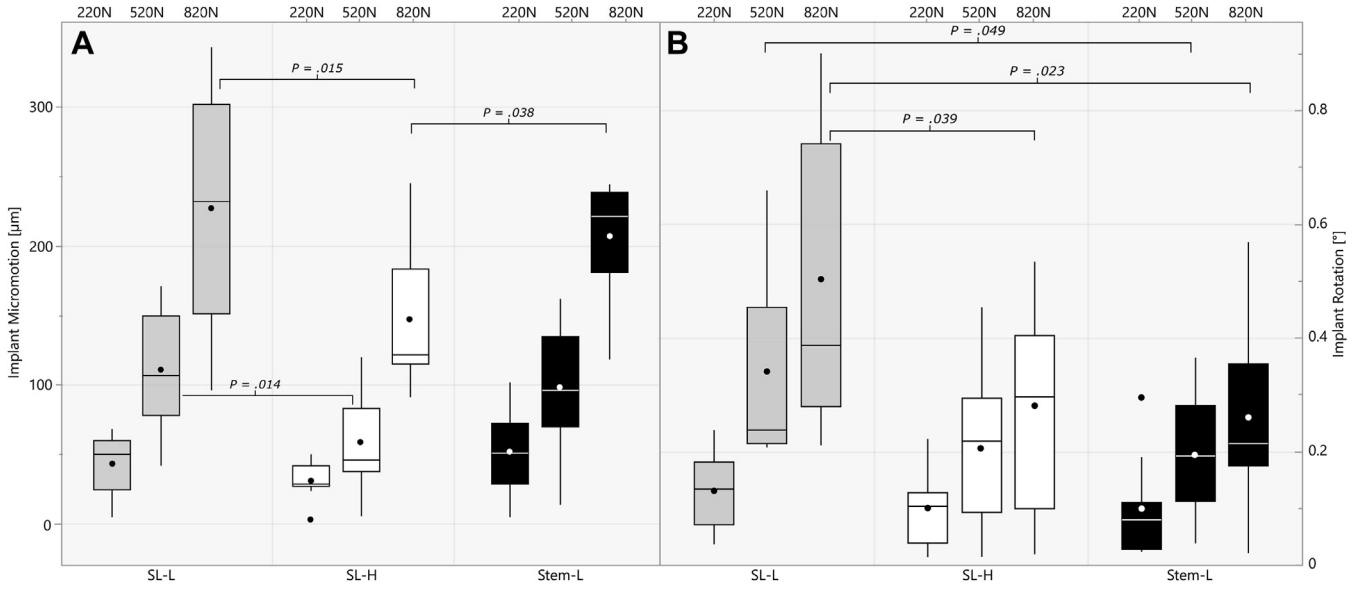

Figure 6 Boxplot of implant translational (**A**) and rotational (**B**) motion during the load hystereses at the end of each cyclic loading block (220 N, 520 N, and 820 N). *SL-L*, stemless implant in low bone density; *SL-H*, stemless implant in high bone density; *Stem-L*, short stem implant in low bone density.

Discussion

The most important finding of this study was that implant–bone compression of a cortical rim-supported stemless implant resulted in increased bone loading at the medial cortex of the proximal humerus, while the press-fit stemmed implant demonstrated improved cyclic rotational and translational stability in low bone density compared to the stemless implant. These outcomes were found to be significantly affected by the amount of loading and the bone density. Significantly increased primary implant stability was found for stemless implants in higher bone densities with the proximal humeral bone providing a reversible

load absorption pattern. Various biomechanical studies of primary implant stability testing are available, but in the current study we additionally investigated humeral implant–bone loading including the assessment of systematically mapped humeral bone densities. Although the in vivo biological effects cannot be reproduced biomechanically such as the effects of bone ingrowth (secondary fixation), stress shielding, and PE wear, this study showed significant differences between current implant types affected by varying bone densities. The experimental findings resulting from investigated superficial cortical bone micromotions caused by different load transfer patterns in the humerus may bridge the gap between FEA simulations and clinical findings.

The behavior of autologous bone is closely linked to the mechanical environment in which osseointegration is intended. Differently maintained mechanical bone stimuli have been reported to have a significant effect on bone restoration, particularly during the proliferative phase of bone healing.[4,5,38] For arthroplasty, micromotions below 150 μm have been reported as the critical threshold for osseointegration with porous-coated implant surfaces.[17,29,30] Within the rehabilitation relevant load levels (220 N, 520 N) the micromotions of all implants were below 150 μm regardless of the cadaveric humeral bone density. While the stemless implant withstood the time-zero 820-N load in higher bone densities, a too-aggressive rehabilitation protocol in lower bone densities may result in significantly increased micromotions (>150 μm) that may prevent bone ingrowth.[3,10,17] Similarly, a biomechanical study using density separation at a BMD of <0.35 g/cm^2 recommended stemmed implants in poorer bone quality for improved stability, except the cortical rim supporting stemless implant may be usable in a wider range of bone densities.[10] The aforementioned stemless implant maintained a homogeneous load transfer to the metaphyseal bone in our study and provided a higher linear stiffness in low and high bone densities under static loading compared to the impacted short-stem implant, confirming a sufficient primary fixation stability and therefore implantability of the implant also in lower bone densities. However, the effect of the implant design on implant stability, implant-bone osseointegration and stress shielding after the time-zero setting can be impaired by various other biological factors influencing trabecular bone formation or resorption[14,32,36,37]

While anatomic stemless implantation is generally considered to be stable, the complication rates remain increased in patients with poor bone density.[9] Therefore, preoperative identification of a patient with low bone density may have implications for the treatment approach. The inferior supporting and metaphyseal periimplant density parameters showed the highest interaction to affect implant stability and bone deformation patterns in this work. Preoperative bone quality assessment may pay off to offer better preoperative knowledge in the surgeons' decision process.[13,22,26,35]

The increased reversible bone deformation observed in our study suggests that a load transfer is maintained in the medial calcar region which may account for the reduced bone resorption in this area observed clinically with a cortical rim support design.[1,2] Recent FE analyses similarly showed a cortical based load transmission through the stemless trunnion supporting implant, mimicking the physiological load pattern in the native humerus.[33,34] Bone load, load frequency and incidence lead to positive bone adaptions in these cases, even though the influences of secondary anchorage due to bone osteointegration at the back of the Calcium Phosphate coated trunnion may influence these findings.[42] Humeral implants without cortical support or more distal load transmission patterns showed bony resorption in impacted stemless and stemmed TSAs respectively.[1,2,25,40] Our findings similarly indicate that the primary stability and bone loading of humeral implants are highly correlated to the design of the device and the respective load transmission at the resection plane. Even though no effects of the bony adaptions on the clinical outcome scores were determined in short-term clinical studies,[1,20,21,23,39] it may affect long-term results, rates of revision cases and periprosthetic fractures.[9,16] Improvements in stress shielding are affirmed by clinical [8,21,24,39] and FEA studies when approximating humeral bone stresses,[12,33,34] although different implant designs seem to have a relevant impact on the bone adaption process. Cortical rim support was shown to decrease the bone density in the cancellous greater tuberosity area, wherefore a cortically supporting design in short stem implants potentially would negatively affect the humeral fixation.[20] Bone loading effects in the metaphyseal cancellous bone were not investigated in this study but may be significantly affected by the use of a cancellous or cortical supporting design. Our study experimentally showed similar behavior of the investigated implants in terms of bone loading and primary implant stability compared to in-silico studies.[12,31,33] Limited activation in either cancellous greater tuberosity or cortical medial calcar areas during the proliferative phase of bone remodeling is associated with reduced mechanical bone stimuli.[15,16] The use of cortically supporting stemless designs may result in improved cortical load transmission and reduced bone resorption at the cortical medial calcar region.

Limitations

We acknowledge some limitations to the current study. Bony ingrowth, which provides secondary anchorage in clinical applications, could not be accounted for in cadaveric biomechanical testing. The stability as well as the load transfer of the investigated implants may behave differently in an in vivo setting over a longer follow-up period. Biological effects and the ability of different implant designs to promote bone ingrowth due to bone loading and implant coatings is a pertinent question that is also beyond the scope of this study. Nevertheless, the findings of this work determined the primary stability of stemless and stemmed implants before bone ingrowth and provided insight into load transfer in an experimental biomechanical study. These findings are important to understand potential causes for stress shielding and implant micromotion which influence postoperative bony integration. Axial compression load was applied in a fixed angle to simulate compressive loading of the humeral head. Bone loading resulting from variable in vivo shoulder joint loading, including rotational and shear forces, may result in different in vivo bone deformations. Thus, the current test methodology is only a rough simulation of the in vivo loading environment and the obtained functional performance could differ from clinical device behavior. Our findings are limited to a stemless cortical rim-supported with screw compression implant and short stem implant. To extend the understanding of different types of bony resorptions, further implants with differing cortical rim support should be investigated with extending the focus from cortical superficial to cancellous observations below the resection plane. Although there is no evidence of bony adaption following stemless reverse shoulder arthroplasty, this approach may also provide important information that will be crucial when testing reverse arthroplasty implant designs.

Conclusion

A cortical rim-supported stemless implant maintained proximally improved dynamic bone loading in variable bone densities compared to a press-fit short stem implant. Biomechanical time-zero implant micromotion in lower bone densities was comparable between short stem and stemless implants at rehabilitation load levels (220 N, 520 N), but with higher cyclic stability and reduced variability for stemmed implantation at daily peak loads (820 N).

Disclaimers:

Funding: Arthrex provided full support of this study.
Conflicts of interest: Daniel Ritter is an employee of Arthrex. Patrick J. Denard receives consulting fees and honoraria from Arthrex, receives support for travel to meetings for the study or other purposes from Arthrex, and receives royalties from Arthrex. Patric Raiss receives consulting fees and honoraria from Arthrex, receives support for travel to meetings for the study or other purposes from Arthrex. Coen A. Wijdicks is an employee of Arthrex. Samuel Bachmaier is an employee of Arthrex. All the other authors, their immediate families, and any research foundations with which they are affiliated have not received any financial payments or other benefits from any commercial entity related to the subject of this article.

References

1. Aibinder WR, Uddin F, Bicknell RT, Krupp R, Scheibel M, Athwal GS. Stress shielding following stemless anatomic total shoulder arthroplasty. Shoulder Elbow 2023;15:54-60. https://doi.org/10.1177/17585732211058804.
2. Alikhah A, Imiolczyk JP, Krukenberg A, Scheibel M. Screw fixation in stemless shoulder arthroplasty for the treatment of primary osteoarthritis leads to less osteolysis when compared to impaction fixation. BMC Musculoskelet Disord 2020;21:295. https://doi.org/10.1186/s12891-020-03277-3.
3. Bachmaier S, Flury M, Lichtenberg S, Schwyzer H-K, Anderl W, Denard PJ, et al. Postpreparation peri-implant humeral bone density and fixation strength vary based on design in stemless reverse shoulder arthroplasty. Semin Arthroplasty JSES 2021;31:677-87. https://doi.org/10.1053/j.sart.2021.04.005.
4. Bailón-Plaza A, Marjolein CH. Beneficial effects of moderate, early loading and adverse effects of delayed or excessive loading on bone healing. J Biomech 2003;36:1069-77. https://doi.org/10.1016/S0021-9290(03)00117-9.
5. Barcik J, Epari DR. Can optimizing the mechanical environment deliver a clinically significant reduction in fracture healing time? Biomedicines 2021;9:691. https://doi.org/10.3390/biomedicines9060691.
6. Bergmann G, Graichen F, Bender A, Kaab M, Rohlmann A, Westerhoff P. In vivo glenohumeral contact forces–measurements in the first patient 7 months postoperatively. J Biomech 2007;40:2139-49. https://doi.org/10.1016/j.jbiomech.2006.10.037.
7. Bergmann G, Graichen F, Bender A, Rohlmann A, Halder A, Beier A, et al. In vivo gleno-humeral joint loads during forward flexion and abduction. J Biomech 2011;44:1543-52. https://doi.org/10.1016/j.jbiomech.2011.02.142.
8. Berth A, Marz V, Wissel H, Awiszus F, Amthauer H, Lohmann CH. SPECT/CT demonstrates the osseointegrative response of a stemless shoulder prosthesis. J Shoulder Elbow Surg 2016;25:e96-103. https://doi.org/10.1016/j.jse.2015.09.009.
9. Casp AJ, Montgomery SRJ, Cancienne JM, Brockmeier SF, Werner BC. Osteoporosis and implant-related complications after anatomic and reverse Total Shoulder Arthroplasty. J Am Acad Orthop Surg 2020;28:121-7. https://doi.org/10.5435/jaaos-d-18-00537.
10. Chen RE, Knapp E, Qiu B, Miniaci A, Awad HA, Voloshin I. Biomechanical comparison of stemless humeral components in total shoulder arthroplasty. Semin Arthroplasty JSES 2022;32:145-53. https://doi.org/10.1053/j.sart.2021.08.003.
11. Churchill RS. Stemless shoulder arthroplasty: current status. J Shoulder Elbow Surg 2014;23:1409-14. https://doi.org/10.1016/j.jse.2014.05.005.
12. Comenda M, Quental C, Folgado J, Sarmento M, Monteiro J. Bone adaptation impact of stemless shoulder implants: a computational analysis. J Shoulder Elbow Surg 2019;28:1886-96. https://doi.org/10.1016/j.jse.2019.03.007.
13. Cronin KJ, Vaughan A, Tzeuton S, Abboud JA. Prospective assessment of osteoporosis in total shoulder arthroplasty. Semin Arthroplasty JSES 2023;33:15-21. https://doi.org/10.1053/j.sart.2022.07.015.
14. Denard PJ, Noyes MP, Walker JB, Shishani Y, Gobezie R, Romeo AA, et al. Proximal stress shielding is decreased with a short stem compared with a traditional-length stem in total shoulder arthroplasty. J Shoulder Elbow Surg 2018;27:53-8. https://doi.org/10.1016/j.jse.2017.06.042.
15. Denard PJ, Raiss P, Gobezie R, Edwards TB, Lederman E. Stress shielding of the humerus in press-fit anatomic shoulder arthroplasty: review and recommendations for evaluation. J Shoulder Elbow Surg 2018;27:1139-47. https://doi.org/10.1016/j.jse.2017.12.020.
16. DeVito P, Judd H, Malarkey A, Elson L, McNeely E, Berglund D, et al. Medial calcar bone resorption after anatomic total shoulder arthroplasty: does it affect outcomes? J Shoulder Elbow Surg 2019;28:2128-38. https://doi.org/10.1016/j.jse.2019.03.017.
17. Favre P, Seebeck J, Thistlethwaite PA, Obrist M, Steffens JG, Hopkins AR, et al. In vitro initial stability of a stemless humeral implant. Clin Biomech 2016;32:113-7. https://doi.org/10.1016/j.clinbiomech.2015.12.004.
18. Filardi V. Stress distribution in the humerus during elevation of the arm and external abduction. J Orthop 2020;19:218-22. https://doi.org/10.1016/j.jor.2020.02.003.
19. Greis M, Heubach K, Hoberg M, Irlenbusch U. Proximal humeral bone loss in stemless shoulder arthroplasty: potential factors influencing bone loss and a new classification system. Arch Orthop Trauma Surg 2022;143:3085-90. https://doi.org/10.1007/s00402-022-04493-3.
20. Habermeyer P, Lichtenberg S, Tauber M, Magosch P. Midterm results of stemless shoulder arthroplasty: a prospective study. J Shoulder Elbow Surg 2015;24:1463-72. https://doi.org/10.1016/j.jse.2015.02.023.
21. Hawi N, Magosch P, Tauber M, Lichtenberg S, Habermeyer P. Nine-year outcome after anatomic stemless shoulder prosthesis: clinical and radiologic results. J Shoulder Elbow Surg 2017;26:1609-15. https://doi.org/10.1016/j.jse.2017.02.017.
22. Hayden A, Cotter EJ, Hennick T, Hetzel S, Wollaeger J, Anderson S, et al. Bone quality in total shoulder arthroplasty: a prospective study correlating CT hounsfield units with thumb test and FRAX score. JSES Int 2023;7:628-35. https://doi.org/10.1016/j.jseint.2023.03.012.
23. Heuberer PR, Brandl G, Pauzenberger L, Laky B, Kriegleder B, Anderl W. Radiological changes do not influence clinical mid-term outcome in stemless humeral head replacements with hollow screw fixation: a prospective radiological and clinical evaluation. BMC Musculoskelet Disord 2018;19:28. https://doi.org/10.1186/s12891-018-1945-6.
24. Huguet D, DeClercq G, Rio B, Teissier J, Zipoli B, Group T. Results of a new stemless shoulder prosthesis: radiologic proof of maintained fixation and stability after a minimum of three years' follow-up. J Shoulder Elbow Surg 2010;19:847-52. https://doi.org/10.1016/j.jse.2009.12.009.
25. Imiolczyk JP, Krukenberg A, Mansat P, Bartsch S, McBirnie J, Gotterbarm T, et al. Midterm results of stemless impaction shoulder arthroplasty for primary osteoarthritis: a prospective, multicenter study. JSES Int 2023;7:1-9. https://doi.org/10.1016/j.jseint.2022.09.001.
26. Levin JM, Rodriguez K, Polascik BA, Zeng S, Warren E Jr, Rechenmacher A, et al. Simple preoperative radiographic and computed tomography measurements predict adequate bone quality for stemless total shoulder arthroplasty. J Shoulder Elbow Surg 2022;31:2481-7. https://doi.org/10.1016/j.jse.2022.05.008.
27. Magosch P, Habermeyer P, Bachmaier S, Metcalfe N. Biomechanische Grundlagen des metaphysär verankerten Humeruskopfersatzes. Obere Extremität 2012;7:11-6. https://doi.org/10.1007/s11678-011-0150-0.
28. Maldonado ZM, Seebeck J, Heller MO, Brandt D, Hepp P, Lill H, et al. Straining of the intact and fractured proximal humerus under physiological-like loading. J Biomech 2003;36:1865-73. https://doi.org/10.1016/s0021-9290(03)00212-4.
29. Peppers T. Fixation of humeral prostheses and axial micromotion. J Shoulder Elbow Surg 1998;7:414-8.
30. Pilliar RM, Lee JM, Maniatopoulos C. Observations on the effect of movement on bone ingrowth into porous-surfaced implants. Clin Orthop Relat Res 1986;208:108-13.
31. Quental C, Folgado J, Fernandes PR, Monteiro J. Bone remodelling analysis of the humerus after a shoulder arthroplasty. Med Eng Phys 2012;34:1132-8. https://doi.org/10.1016/j.medengphy.2011.12.001.
32. Raiss P, Edwards TB, Deutsch A, Shah A, Bruckner T, Loew M, et al. Radiographic changes around humeral components in shoulder arthroplasty. J Bone Joint Surg Am 2014;96:e54. https://doi.org/10.2106/JBJS.M.00378.
33. Razfar N, Reeves JM, Langohr DG, Willing R, Athwal GS, Johnson JA. Comparison of proximal humeral bone stresses between stemless, short stem, and standard stem length: a finite element analysis. J Shoulder Elbow Surg 2016;25:1076-83. https://doi.org/10.1016/j.jse.2015.11.011.
34. Reeves JM, Langohr GDG, Athwal GS, Johnson JA. The effect of stemless humeral component fixation feature design on bone stress and strain response: a finite element analysis. J Shoulder Elbow Surg 2018;27:2232-41. https://doi.org/10.1016/j.jse.2018.06.002.
35. Ritter D, Denard PJ, Raiss P, Wijdicks CA, Bachmaier S. Preoperative 3D computed tomography bone density measures provide objective bone quality classifications for stemless anatomic total shoulder arthroplasty. J Shoulder Elbow Surg 2024. https://doi.org/10.1016/j.jse.2023.11.005.
36. Sandberg OH, Aspenberg P. Inter-trabecular bone formation: a specific mechanism for healing of cancellous bone. Acta Orthop 2016;87:459-65. https://doi.org/10.1080/17453674.2016.1205172.
37. Schnetzke M, Coda S, Raiss P, Walch G, Loew M. Radiologic bone adaptations on a cementless short-stem shoulder prosthesis. J Shoulder Elbow Surg 2016;25:650-7. https://doi.org/10.1016/j.jse.2015.08.044.
38. Ulstrup AK. Biomechanical concepts of fracture healing in weight-bearing long bones. Acta Orthop Belg 2008;74:291-302.
39. Uschok S, Magosch P, Moe M, Lichtenberg S, Habermeyer P. Is the stemless humeral head replacement clinically and radiographically a secure equivalent to standard stem humeral head replacement in the long-term follow-up? A prospective randomized trial. J Shoulder Elbow Surg 2017;26:225-32. https://doi.org/10.1016/j.jse.2016.09.001.
40. Vegas A, Cannon D, Lewis S, Glener J, Mekkawy KL, Rodriguez HC, et al. Impact of humeral stem length on calcar resorption in anatomic total shoulder arthroplasty. J Shoulder Elbow Surg 2023;33:130-8. https://doi.org/10.1016/j.jse.2023.05.033.
41. Westerhoff P, Graichen F, Bender A, Halder A, Beier A, Rohlmann A, et al. In vivo measurement of shoulder joint loads during activities of daily living. J Biomech 2009;42:1840-9. https://doi.org/10.1016/j.jbiomech.2009.05.035.
42. Wolff J. Das Gesetz der Transformation der Knochen. Dtsch Med Wochenschr 1893;19:1222-4. https://doi.org/10.1055/s-0028-1144106.